Effects of lithographic parameters in massively parallel electron-beam systems

Soomin Moon, Soo-Young Lee, Jin Choi, Seom-Beom Kim, and Chan-Uk Jeon

Citation: Journal of Vacuum Science & Technology B **36**, 06JA03 (2018); doi: 10.1116/1.5048084
View online: https://doi.org/10.1116/1.5048084
View Table of Contents: http://avs.scitation.org/toc/jvb/36/6
Published by the American Vacuum Society

Effects of lithographic parameters in massively parallel electron-beam systems

Soomin Moon,[1] Soo-Young Lee,[1,a)] Jin Choi,[2] Seom-Beom Kim,[2] and Chan-Uk Jeon[2]
[1]*Department of Electrical and Computer Engineering, Auburn University, Auburn, Alabama 36849*
[2]*Samsung Electronics, Mask Development Team, 16 Banwol-Dong, Hwasung, Kyunggi-Do 445-701, Korea*

(Received 11 July 2018; accepted 17 October 2018; published 7 November 2018)

The ability of electron-beam (e-beam) lithography to transfer fine features onto a substrate is essential in many applications where high-resolution devices need to be fabricated. However, its low throughput has been the major drawback, especially for transferring large-scale patterns such as optical masks. In order to overcome the drawback, e-beam machines with massively parallel beams were recently developed and their throughput improved by several orders of magnitude has been experimentally demonstrated. In this study, for the optimal use of such parallel-beam systems, the effects of lithographic parameters and faulty beams on the writing quality are analyzed. The metrics of writing quality include the exposure variation and contrast, the total dose required, the dose latitude, and the line edge roughness. The analysis results obtained through an extensive simulation are provided and discussed in this paper. *Published by the AVS.* https://doi.org/10.1116/1.5048084

I. INTRODUCTION

Electron-beam (e-beam) lithography has a capability of transferring a fine-feature pattern onto a substrate and is widely utilized in various applications of pattern transfer.[1–5] However, its main drawback of low throughput has become a limiting factor for large-scale patterns as the pattern size and complexity continue to increase. In response to the need for significant improvement of writing throughput, there have been many efforts to develop e-beam systems which utilize multiple beams.[6–10] Some of those efforts recently lead to fruitful outcomes, new e-beam systems with massively parallel beams. While the throughput improved by several orders of magnitude has been demonstrated,[6,9] there is a need for analyzing the writing quality in order to enable the optimal use of such systems. In this study, the dependency of writing quality on lithographic parameters has been examined.

In a massively parallel e-beam system, each beam can be considered to be a shaped beam of which the shape is dependent on the aperture and is fixed. First, due to the beam blur along the boundary of a beam and electron scattering in the resist,[11] the spatial distribution of exposure (energy deposited in the resist) within a feature may not be uniform even when all points in the feature are exposed with a constant dose. Second, the number of bits used to encode a dose level for each beam may be limited to reduce the required rate of data transfer into the e-beam control unit.[12] As a way to increase the dose resolution, each point (pixel) on the resist surface may be allowed to be exposed by multiple beams in an overlapping manner. That is, the exposing interval can be smaller than the pixel interval (size), which makes slower the exposure change over the feature boundary. Third, it is possible that some beams may become faulty and are not able to give a specified level of dose to certain pixels. Though the faulty rate must be very low, the effect of faulty beams, i.e., the exposure reduction at a pixel or pixels, may not be negligible.

The abovementioned effects can cause a substantial change in the spatial distribution of exposure and therefore the writing quality. Through an extensive simulation, the writing quality such as exposure variation and contrast, total dose, line edge roughness (LER), maximum indent, and dose latitude is analyzed in terms of lithographic parameters such as the exposing interval, etc., as a first step toward the development of a method to optimally utilize an e-beam system with massively parallel beams. The results indicate that the effects can be substantial and therefore need to be taken into account.

There are other parameters representing nonideal conditions which cause a deviation from the ideal or desired distribution of exposure, such as the fluctuating current density, the variation of aperture size, and the position error of beams. However, this study focuses on the exposing interval, the beam shape, and a faulty beam only. That is, the results reported in this paper are what can happen even when such nonideal conditions do not exist.

In Sec. II, a model of the massively parallel e-beam system is described. In Sec. III, the metrics of writing quality are introduced. In Sec. IV, the simulation study is described. In Sec. V, the results are presented and discussed, followed by a summary in Sec. VI.

II. MODEL OF THE MASSIVELY PARALLEL SYSTEM

In a massively parallel system like the electron multi-beam mask exposure tool,[6–8] a large number of beams is generated through a 2D array of aperture, each of which defines a beam. The beam size and interval are adjusted by electronic lenses before beams reach a substrate. While beams can be individually turned on and off, the deflection of beams, which may be needed in a certain writing strategy, is executed in a synchronized manner, i.e., the same deflection angle for all beams. The analysis in this study focuses on the

a)Electronic mail: leesooy@eng.auburn.edu

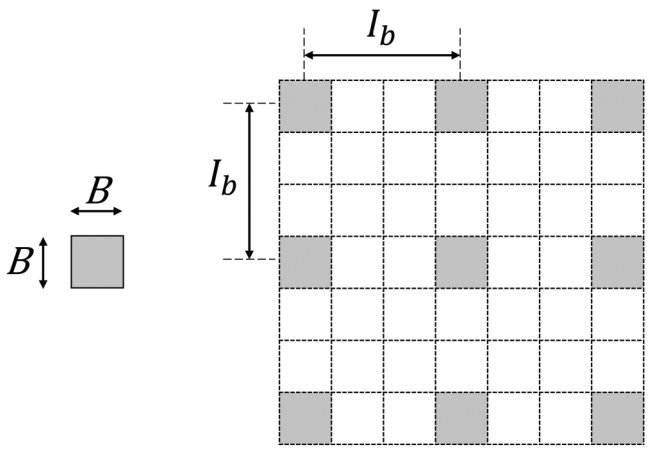

FIG. 1. Each beam is shaped through a square aperture and the size of the beam at the resist surface is $B \times B$. An illustration of beam array is provided where $I_b = 3B$.

exposure distribution in the resist and its effects on the writing quality. Therefore, the beams arriving at the surface of resist are of interest regardless of the processes of their generation, adjustment, and control.

In Fig. 1, a 2D array of beams at the surface of resist is illustrated where a square aperture is assumed. The beam size is $B \times B$ and the beam interval is I_b in both dimensions. Normally, I_b is significantly larger than B in a massively parallel system. In most cases, the spatial variation of exposure within a feature due to the gap between adjacent beams needs to be avoided. A writing strategy may adjust the on–off frequency of beams as the substrate moves under the parallel beams such that the distance between two adjacent points exposed is less than I_b. The distance between two adjacent exposed points is referred to as exposing interval, I_e, in both dimensions. The directly exposed regions of size $B \times B$ may overlap depending on B and I_e as shown in Fig. 2.

Each beam may be considered as a shaped beam where the (cross section) shape is determined by the aperture and is assumed to be of square in this study. The beam blur occurs as a beam goes through the aperture and travels down from the electron source to the resist surface.[11] Also, electrons experience the scattering in the resist. Therefore, the spatial distribution of exposure contributed by a beam shows a certain degree of blurring over the beam boundary. The spatial distribution of exposure contributed from a shaped beam is referred to as *transfer function* to be distinguished from a point spread function. The transfer function is modeled to be flat at its center and decreases over its boundary. The decrease follows a Gaussian function such that the peak of Gaussian function equals the exposure in the flat region and the exposure at the boundary is a half of the peak. The sharpness of transfer function is controlled by the standard deviation σ of Gaussian function, which is referred to as *blurring factor*. An example of transfer function is shown in Fig. 3.

III. QUALITY METRICS

In analyzing the writing quality, a few metrics are considered, i.e., exposure variation within a feature, exposure contrast over the feature boundary, line edge roughness, total dose, dose latitude, etc. In the analysis, a feature of single line is considered which is exposed by parallel beams where the dose is constant for all beams. The notations below are adopted in this paper:

x: the width dimension of a feature
y: the length dimension of a feature
z: the resist-depth dimension
W: the width of a feature
L: the length of a feature
$d(x, y)$: the dose distribution
$e(x, y, z)$: the exposure distribution in the resist
$t(x, y, z)$: the transfer function

The 3D exposure distribution in the resist may be computed through the discrete convolution as in Eq. (1)

$$e(x, y, z) = \sum_{x'} \sum_{y'} d(x', y') t(x - x', y - y', z), \tag{1}$$

where $d(x, y)$ specifies the spatial distribution of the dose given by all beams.

A. Exposure variation

In general, it is desired that the spatial variation of exposure within each feature is minimal since the variation causes an uneven development of resist and may lead to a rough

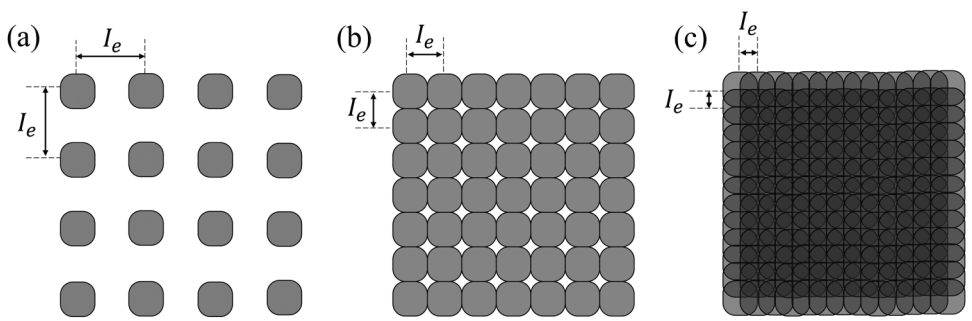

FIG. 2. Exposing interval I_e varies depending on the writing strategy: (a) $I_e > B$ where $I_e = 2B$, (b) $I_e = B$ and (c) $I_e < B$ where $I_e = B/2$.

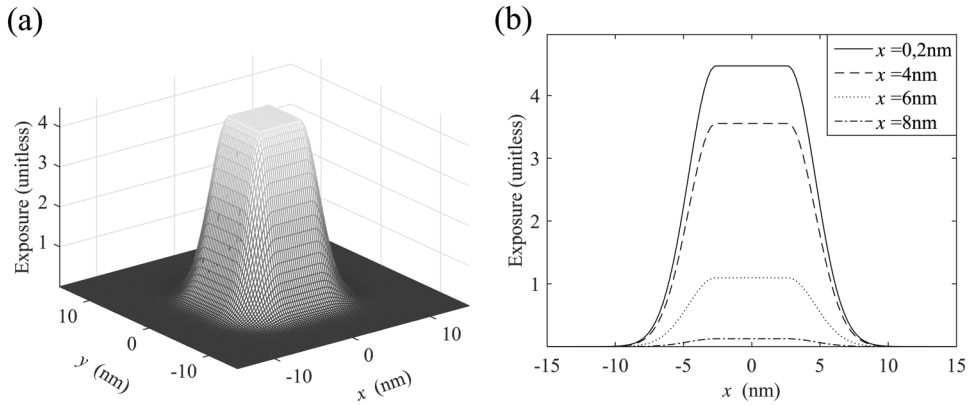

FIG. 3. (a) 3D view and (b) cross section of the transfer function with $B = 10$ nm and $\sigma = 2$ nm.

boundary of a feature. The exposure variation may be quantified as the standard deviation of exposure within a feature at a certain resist layer, $z = z_i$ (refer to Fig. 4).

$$\sigma_e = \sqrt{\frac{1}{WL}\sum_{y=0}^{L}\sum_{x=0}^{W}[e(x, y, z_i) - \overline{e}(z_i)]^2}, \tag{2}$$

where $\overline{e}(z_i) = (1/WL)\sum_{y=0}^{L}\sum_{x=0}^{W} e(x, y, z_i)$.

Such quantification can be dominated by the exposure drop over the boundary of a feature, especially when the drop occurs over a significant distance as shown in Fig. 4. Therefore, another measure of exposure variation may be considered, which excludes the exposure drop over the feature boundary, shown as exposure fluctuation in Fig. 4. The exposure variation is analyzed in this study.

B. Exposure contrast

When a feature is exposed with a uniform dose, the exposure is high in the interior region of the feature and decreases toward and over the feature boundary. The exposure contrast is typically defined as the exposure change over the feature boundary. The exposure may fluctuate spatially and, therefore, the exposure contrast at a certain layer, $z = z_i$, is defined as the difference between the exposure averages over multiple points inside and outside a feature as in Eq. (3) (refer to Fig. 5).

$$C_e = \frac{1}{n_c L}\sum_{y=0}^{L}\left|\sum_{x=0}^{n_c-1} e(x, y, z_i) - \sum_{x=-n_c}^{-1} e(x, y, z_i)\right|, \tag{3}$$

where n_c is the number of points over which the exposure average is computed ($n_c = 4$ in Fig. 5) and $x = 0$ corresponds to the feature boundary.

The higher the exposure contrast is, the more stable the feature boundary tends to be during the development process. The main factor affecting the exposure contrast is the shape of the transfer function. Given a transfer function, the exposing interval I_e, e.g., overlapping between the

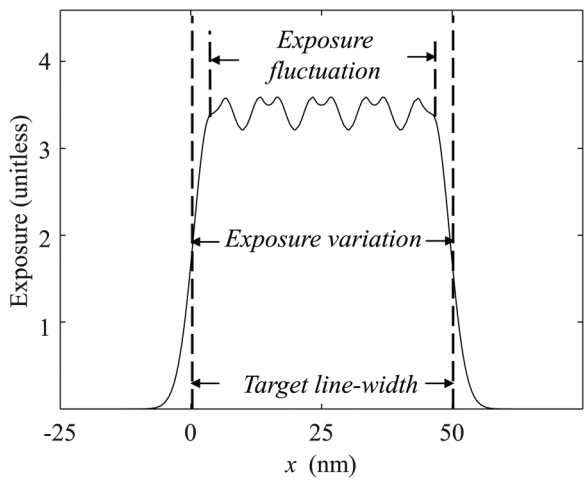

FIG. 4. Exposure variation is computed within the target line-width and the exposure fluctuation refers to the exposure variation excluding the large change of exposure over the feature edges. $I_e = B = 10$ nm, $W = 50$ nm, and $\sigma = 3$ nm.

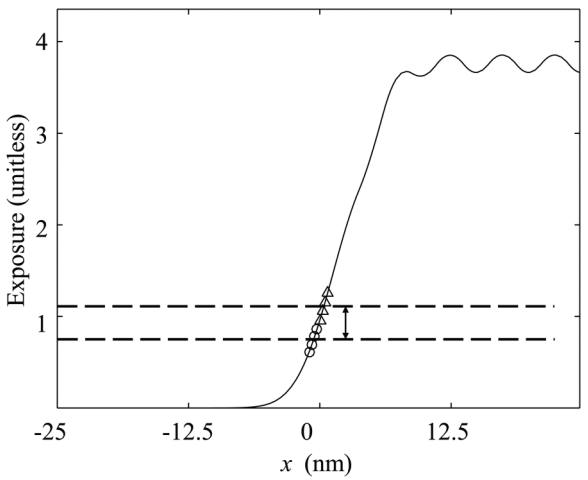

FIG. 5. Exposure contrast is computed as the difference of the exposure averages evaluated at multiple points inside and outside a feature. In this illustration, $x = 0$ corresponds to the feature edge and the exposures at four points each inside (triangle) and outside (circle) are involved. $B = 10$ nm, $I_e = 5$ nm, $W = 50$ nm, and $\sigma = 3$ nm.

domains of beams, can also affect the exposure contrast as illustrated in Fig. 5.

C. Total dose

A higher dose usually makes a larger area of resist developed for a given developing time. However, it is possible that two different total doses may lead to the same size of the feature after the development, depending on the exposure distribution. From the viewpoint of reducing the writing time, a lower total dose would be preferred. Hence, the total dose, D_t, required for a unit-length segment of a line to develop to the target line-width is considered in this study. When the beam size is $B \times B$ and the exposing interval is I_e, $(W - B/I_e) + 1$ beams can fit over the line-width of W. Along the length dimension of the line, $1/I_e$ beams can fit over a unit-length. Then, D_t is derived as in Eq. (4).

$$D_t = \frac{d}{I_e}\left(\frac{W - B}{I_e} + 1\right), \tag{4}$$

where d is the dose per beam required to achieve the target line-width (note that d varies with I_e).

D. Line edge roughness

The roughness of the feature boundary is mainly caused by the stochastic exposure fluctuation and the developing process. Another possible source of boundary roughness is the systematic variation in the spatial distribution of exposure, caused by the shape of transfer function and exposing interval. Also, faulty beams may introduce localized drops in the spatial distribution of exposure, which can contribute to the roughness. In this study, the LER due to the systematic exposure variation and faulty beams is analyzed. The LER is quantified as the standard deviation of edge location in a line feature, which can be expressed as follows (refer to Fig. 6):

$$\mathrm{LER} = \sqrt{\frac{1}{L}\sum_{y=0}^{L}(x_e(y) - \bar{x}_e)^2}, \tag{5}$$

where $x_e(y)$ is the edge location and $\bar{x}_e$ is the average edge location, i.e., $\bar{x}_e = (1/L)\sum_{y=0}^{L} x_e(y)$ at a resist layer.

Along with the LER, the maximum indent (see Fig. 6) is also a meaningful metric, which can cause a bottle-neck increasing the resistance of a signal path. The maximum indent is measured as the distance from the average edge location to the farthest edge point inward. That is, the maximum indent $(\Delta x_e)_{max}$ can be represented as

$$(\Delta x_e)_{max} = \max_y (\,|\, x_e(y) - \bar{x}_e \,|\,). \tag{6}$$

It needs to be pointed out that the LER and maximum indent considered in this study do not include the boundary roughness caused by the randomness in the exposure and developing processes. Only the boundary roughness due to the periodic variation of exposure determined by the transfer function and lithographic parameters is considered, i.e., the roughness one may get even when the exposing and developing processes are deterministic.

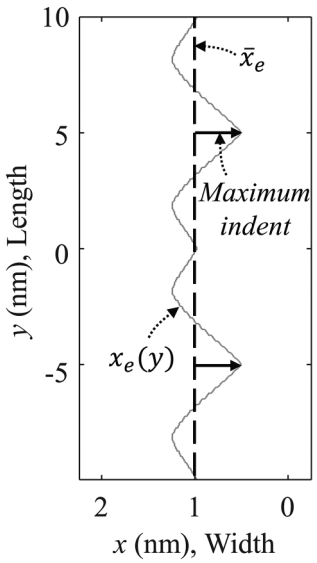

FIG. 6. LER is computed as the standard deviation of edge location $x_e(y)$ (solid) and the maximum indent is the largest distance inward to the edge from the average edge location $\bar{x}_e$ (dashed). In this illustration, the left boundary of a line feature is shown. B = 10 nm, I_e = 10 nm, W = 30 nm, and σ = 3 nm.

E. Dose latitude

As the dose level varies, the critical dimension (CD), e.g., line-width, of a feature changes. The sensitivity of CD to the dose level is referred to as dose latitude which may be defined as the dose variation causing the $\pm 2\%$ variation of CD. Given a substrate system and a developing process, the dose latitude is mainly determined by the spatial distribution of exposure, which in turn depends on the lithographic parameters.

The dose latitude is computed as follows:

$$\text{dose latitude} = \frac{d_{102} - d_{98}}{d_{100}} \times 100\%, \tag{7}$$

where d_{98}, d_{100}, and d_{102} are the doses required to develop the 98%, 100%, and 102% of the target CD, respectively.

IV. SIMULATION

A single line is exposed by a massively parallel e-beam system along its length dimension on a typical substrate system. The 3D exposure distribution in the resist is computed at the resolution, I_s, referred to as *simulation interval* where $I_s < I_e$ to be able to consider the detail of exposure distribution as shown in Fig. 7. In this study, I_s is set to $I_e/4$. The resist is modeled by five layers to take into account the layer dependency of exposure and at the same time avoid too long a simulation time. From the exposure distribution, the exposure variation and contrast are computed. The developing-rate

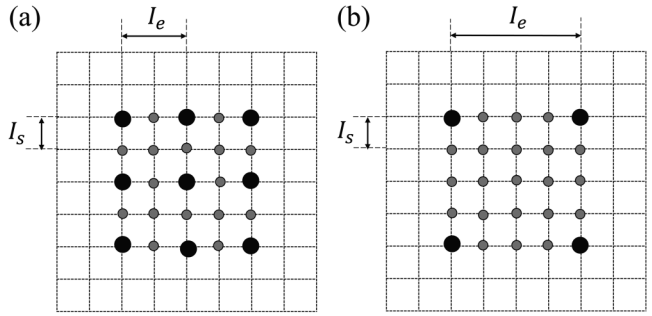

FIG. 7. In the simulation, the exposure is evaluated at a finer resolution (I_s) than the exposing interval (I_e): (a) $I_s = I_e/2$ and (b) $I_s = I_e/4$. The dark points are exposed and the exposure is computed at both dark and gray points.

distribution is derived from the exposure distribution and then the remaining resist profile is obtained through a resist development simulation.[13] The development simulation continues until the line feature is fully developed to the bottom layer of resist. From the resist profile, the maximum indent and LER are quantified. The total dose required and dose latitude can be found by repeating the development simulation.

The aperture is assumed to be a square as in the currently available systems, and the beam cross section at the surface of resist is 10 nm × 10 nm (B = 10 nm). The exposing interval is varied from 1 to 10 nm and the blurring factor of transfer function from 1 to 4 nm. The simulation interval is 0.25 nm. The line feature is 150 nm long and the middle 60% segment is used in the computation of the metrics to exclude the edge effect (corner rounding). The three different line-widths, 30, 50, and 100 nm, are considered. The above simulation procedure is repeated for every possible combination of lithographic parameters.

The transfer function which describes the spatial distribution of exposure in the resist contributed by a beam is modeled based on the point spread function generated using a Monte Carlo simulation program SEEL (Ref. 14) for the substrate system of 100 nm PMMA on Si and the beam energy of 50 keV. From the point spread function, the total exposure and forward scattering range (the standard deviation of Gaussian) are extracted in each resist layer. The ratios of the total energy and forward scattering range among the five resist layers are referred to in defining the transfer function. Then, the blurring factor for the middle layer is varied in the simulation (i.e., the blurring factors for the other layers are accordingly determined).

For the size of the feature used in this study, a relatively small number of beams is needed to expose the feature. Therefore, in the simulation of faulty beams, the effect of a single faulty beam, rather than the effect of a faulty rate, is considered. Note that the faulty rate is usually very low in a massively parallel system and the number of faulty beams is likely to be 0 for a small number of beams.

V. RESULTS AND DISCUSSION

The simulation results for the system with no faulty beam are presented first, followed by the results for a faulty system. All of the quality metrics are evaluated, according to the respective equations in Sec. III, at the bottom layer of resist to ensure that the feature is fully developed. Note that the metrics would show the similar tendencies at other layers.

A. Exposure contrast

The exposure contrast (refer to Eq. 3) is analyzed as a function of the exposing interval and the blurring factor. The results for three line-widths are provided in Table I. The exposure contrast is larger for a larger exposing interval. A smaller exposing interval results in a larger overlap between the (directly exposed) regions of adjacent points (refer to Fig. 1). The larger the overlap is, the more gradually the exposure varies over the boundary of a feature due to a higher level of smoothing. Note that such smoothing does not occur when $I_e = B$, i.e., no overlap. The exposure contrast is smaller for a larger blurring factor (σ). The transfer function with a larger blurring factor decreases slower from its maximum, leading to a smaller change of exposure over the feature boundary. The line-width does not affect the exposure contrast. The exposure distribution over the feature boundary is not dependent on the feature size as long as the beam size, B, is smaller than the feature size.

B. Exposure variation

The spatial variation of exposure within the feature (refer to Eq. 2) is provided in Table II. The exposure variation is smaller for a larger exposing interval (when $I_e \leq B$). When the exposing interval is smaller, the exposure drops gradually from the maximum level of the flat (plateau) region over a longer distance to a lower level, compared to the case of a larger exposing interval as can be seen in Fig. 8. This makes the exposure variation larger. The exposure variation decreases as the blurring factor increases when the

TABLE I. Exposure contrast for the line-width (W) of (a) 30 nm, (b) 50 nm, and (c) 100 nm: the exposure contrast is normalized to the average exposure within the line.

	σ (nm)			
I_e (nm)	1	2	3	4
(a)				
1	0.10	0.087	0.081	0.078
2	0.14	0.10	0.091	0.085
5	0.30	0.16	0.12	0.10
10	0.50	0.28	0.19	0.15
(b)				
1	0.087	0.074	0.069	0.066
2	0.12	0.09	0.079	0.073
5	0.27	0.15	0.11	0.095
10	0.49	0.27	0.18	0.14
(c)				
1	0.078	0.066	0.062	0.059
2	0.11	0.082	0.071	0.066
5	0.26	0.14	0.10	0.088
10	0.49	0.27	0.18	0.14

exposing interval is relatively smaller. When the exposing interval is smaller, the flat region is narrower and the exposure difference between the flat region and feature boundary is larger. As the blurring factor increases, the exposure distribution tends to spread, making the exposure difference and therefore the exposure variation smaller. However, when the exposing interval is larger, the exposure-spreading effect due to the increased blurring factor diminishes. On the other hand, the exposure fluctuation (see Fig. 4) increases with the blurring factor, which eventually makes the exposure variation increase as seen in the case of $I_e = B$.

The exposure variation is smaller for a larger feature (line-width). The relative size of the flat region (compared to the feature size) is larger and the effect of the exposure drop in the boundary region becomes relatively less as the feature size increases. That leads to a smaller exposure variation. Also, the relative exposure fluctuation (compared to the average exposure level) becomes smaller for a larger feature.

If I_e is increased beyond B, the exposure fluctuation becomes dominant, compared to the exposure drop in the boundary region. The exposure fluctuation increases as the exposing interval increases while $I_e > B$. Therefore, the exposure variation would increase with I_e (unless $I_e \gg B$).

C. Total dose

The total dose required to achieve the target line-width at the bottom layer is examined for three line-widths [refer to Eq. (4)] and the results are provided in Table III. Except for the line-width of 30 nm, the total dose increases as the exposing interval decreases or the blurring factor decreases in the case of $I_e = 1$ nm. A smaller exposing interval, or a smaller blurring factor with a small exposing interval, results in a narrower flat region in the exposure distribution and a larger exposure difference between the flat and boundary regions. With such an exposure distribution, the resist needs to be developed faster vertically in the flat region to reach the target boundary at the bottom layer through the lateral development. A relatively longer time is spent in the lateral development than in the vertical development due to the less-balanced spatial distribution of exposure. In such a case, the dose is less effectively utilized for the resist development and, therefore, a higher total dose is required.

However, when the feature size is smaller, the aspect ratio, i.e., the ratio of resist thickness to feature size, is larger and a relatively less lateral development is needed. Hence, a less-balanced spatial distribution of exposure, where the exposure is higher at the center of a feature and decreases toward the feature boundary, does not lead to a lower efficiency in the resist development. This explains why the total

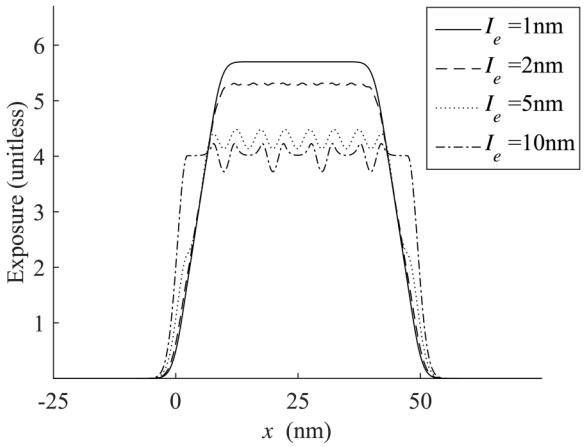

FIG. 8. Exposure distribution along the width dimension at the middle layer of resist. B = 10 nm, W = 50 nm, and σ = 2 nm.

TABLE II. Exposure variation for the line-width (W) of (a) 30 nm, (b) 50 nm, and (c) 100 nm: the exposure variation is normalized to the average exposure within the line.

	σ (nm)			
I_e (nm)	1	2	3	4
(a)				
1	0.45	0.44	0.43	0.41
2	0.41	0.40	0.39	0.38
5	0.29	0.30	0.30	0.29
10	0.099	0.12	0.14	0.16
(b)				
1	0.35	0.35	0.34	0.33
2	0.32	0.32	0.31	0.31
5	0.23	0.24	0.24	0.23
10	0.085	0.098	0.12	0.14
(c)				
1	0.24	0.24	0.24	0.24
2	0.22	0.22	0.22	0.22
5	0.17	0.17	0.17	0.17
10	0.072	0.078	0.091	0.12

TABLE III. Total dose for the line-width (W) of (a) 30 nm, (b) 50 nm, and (c) 100 nm: the total dose is normalized to the lowest total dose required.

	σ (nm)			
I_e (nm)	1	2	3	4
(a)				
1	1.09	1.06	1.04	1.03
2	1.02	1.04	1.04	1.04
5	1.00	1.00	1.04	1.08
10	1.07	1.08	1.09	1.09
(b)				
1	1.20	1.17	1.14	1.13
2	1.09	1.12	1.12	1.11
5	1.01	1.01	1.05	1.09
10	1.00	1.01	1.03	1.02
(c)				
1	1.33	1.30	1.27	1.25
2	1.20	1.23	1.22	1.22
5	1.07	1.07	1.11	1.16
10	1.00	1.01	1.03	1.02

dose does not increase with the exposing interval decreased when the line-width is 30 nm.

D. Dose latitude

The dose latitude [refer to Eq. (7)] is provided for three line-widths in Table IV. When the average exposure levels in the flat and boundary regions are the same or similar between two cases, the dose latitude is larger in the cases where the exposure contrast is larger. This explains the observation that the dose latitude is larger for a smaller blurring factor with the exposing interval fixed. Another factor affecting the dose latitude is the exposure difference between the flat and boundary regions (see Fig. 8). When the exposure difference is larger, the edge location is affected less by the exposure distribution in the boundary region. Therefore, as the dose changes, the edge location moves less, i.e., a larger dose latitude. When the exposing interval increases, the exposure contrast increases, but the exposure difference decreases. The reason why the dose latitude is smaller for a larger exposing interval is that the effect of the exposure difference is larger than that of the exposure contrast.

E. LER and maximum indent

The LER and maximum indent [refer to Eqs. (5) and (6)] measured along the length dimension for the line-width of 50nm are provided in Table V. A typical source of LER is the stochastic fluctuation of exposure. However, as pointed out earlier, the LER and maximum indent in Table V are the ones due to the periodic variation of deterministic exposure. Such variation can be substantial depending on the shape of transfer function and exposing interval. It is seen that the LER and maximum indent are small but not negligible. They decrease as the exposing interval decreases since the exposure distribution tends to be smoothed out. The largest LER and maximum indent are obtained when both exposing interval and blurring factor are largest. This is because the exposure fluctuation is maximized in that case.

TABLE IV. Percent dose latitude (%) for the line-width (W) of (a) 30 nm, (b) 50 nm, and (c) 100 nm: the dose latitude is computed relative to the dose required to achieve the target line-width.

	σ (nm)			
I_e (nm)	1	2	3	4
(a)				
1	14.94	9.43	6.92	5.21
2	9.34	6.80	5.15	4.25
5	3.68	3.35	3.00	2.65
10	1.36	1.50	1.46	1.47
(b)				
1	28.34	16.32	11.18	8.67
2	16.83	11.57	8.87	6.23
5	6.65	5.71	5.08	4.36
10	2.60	2.59	2.46	2.46
(c)				
1	106.58	36.11	24.74	18.77
2	54.57	25.93	19.05	15.29
5	19.87	12.41	11.20	9.45
10	8.99	5.82	5.17	5.07

TABLE V. (a) LER and (b) maximum indent in nm for the line-width (W) of 50 nm.

	σ (nm)			
I_e (nm)	1	2	3	4
(a)				
1	0	0	0	0
2	0.039	0.020	0.0095	0
5	0.11	0.18	0.17	0.028
10	0.35	0.34	0.43	0.62
(b)				
1	0	0	0	0
2	0.053	0.029	0.021	0
5	0.25	0.29	0.29	0.057
10	0.94	0.72	0.96	1.14

F. Faulty beam

One of the factors determining how a faulty beam affects the writing quality is the location of the point exposed by the faulty beam. The effect would be larger when the point is closer to the feature boundary. Also, the effect of a faulty beam may vary significantly depending on the writing redundancy and exposing interval. The writing redundancy refers to the number of beams jointly exposing a point,[7,8] e.g., two-beam redundancy corresponds to the case where each point is exposed by two different beams. In Table VI, the LER and maximum indent are provided for the cases of one faulty beam. It is first observed that a faulty beam can affect the writing quality substantially, especially when an edge point is exposed by the faulty

TABLE VI. LER and maximum indent with the redundancy varied for the line-width (W) of 50 nm (a) when the faulty beam exposes points in the middle of the feature and (b) when the faulty beam exposes points on the feature boundary: I_e = 10 nm and σ = 2 nm. The LER and maximum indent when no beam is faulty are also included for reference.

	LER (nm)				Maximum indent (nm)			
		Redundancy				Redundancy		
I_e (nm)	No fault	1	2	4	No fault	1	2	4
(a)								
1	0	0	0	0	0	0	0	0
2	0.020	0.028	0.023	0.019	0.029	0.052	0.039	0.031
5	0.18	0.21	0.19	0.19	0.29	0.43	0.36	0.34
10	0.34	0.41	0.39	0.39	0.72	1.06	1.12	1.14
(b)								
1	0	0	0	0	0	0	0	0
2	0.020	0.041	0.026	0.021	0.029	0.082	0.047	0.037
5	0.18	0.69	0.43	0.30	0.29	1.05	0.86	0.61
10	0.34	2.02	1.86	1.24	0.72	4.16	3.58	3.47

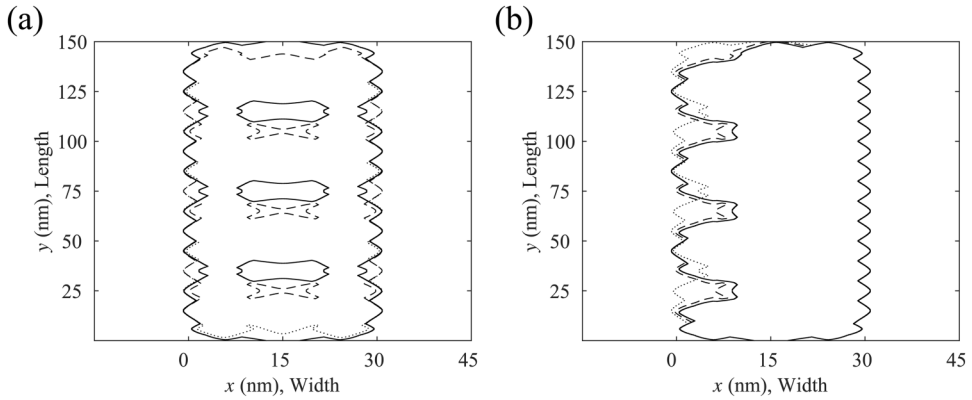

FIG. 9. Contour of the remaining resist profile for the line-width (W) of 30 nm: (a) when center points are exposed by a faulty beam and (b) left edge points are exposed by a faulty beam. It is assumed that a point receives no dose from a faulty beam. $B = I_e = 10$ nm and $\sigma = 4$ nm. The contours for the 1-beam, 2-beam, and 4-beam redundancies are indicated by the solid, dashed, and dotted curves, respectively.

beam. When a point in the middle of a feature receives a lower exposure due to a faulty beam, the isotropic development of resist can mitigate the effect of lower exposure on the final feature boundary through the developing process. However, in the case of a lower exposure on an edge point, such mitigation would be minimal since the edge points are developed in the final stage of resist development. Also, it is seen that the effects on the LER and maximum indent are smaller for a higher writing redundancy and a smaller exposing interval. This is due to the fact that the exposure drop due to a faulty beam is smaller when a point is exposed by a larger number of beams (i.e., a higher writing redundancy) or the exposing interval is smaller leading to a larger overlapping between the domains of two adjacent beams on the resist surface.

In Fig. 9, the contours of remaining resist profile are shown with the writing redundancy varied. It can be seen that the boundary roughness, in particular the maximum indent, is larger for a smaller writing redundancy and the effect of a faulty beam is maximized when it exposes edge points [see Fig. 9(b)].

VI. SUMMARY

The inherent drawback of an e-beam lithographic system has been its low throughput due to the use of a single beam. The main effort to improve the throughput by orders of magnitude has been to employ multiple beams in a system. As a result, e-beam systems with massively parallel beams were recently developed. To maximize the efficiency of such a system, it is critical to utilize the parallel beams in an optimal way. As a first step, this study investigates the effects of the lithographic parameters on the writing qualities. The lithographic parameters such as the exposing interval, blurring factor, writing redundancy, etc. are considered, and the quality metrics, including the exposure variation and contrast, total dose required, dose latitude, and line edge roughness are analyzed. Through an extensive simulation, it has been shown that the effects on most of the metrics can be substantial, which warrants a further investigation. Though the quantitative results may vary depending on the simulation set-up, the behaviors of the quality metrics are likely to be similar with those reported in this paper. Based on the analysis results, it will be attempted to develop effective guidelines for the optimal use of a massively parallel e-beam system.

ACKNOWLEDGMENT

This work was supported in part by a research grant from Samsung Electronics Co., Ltd.

[1]S.-Y. Lee and B. D. Cook, IEEE Trans. Semicond. Manuf. **11**, 117 (1998).
[2]U. Hofmann, R. Crandall, and L. Johnson, J. Vac. Sci. Technol. B **17**, 2940 (1999).
[3]M. Osawa, K. Takahashi, M. Sato, H. Arimoto, K. Ogino, H. Hoshino, and Y. Machida, J. Vac. Sci. Technol. B **19**, 2483 (2001).
[4]S.-Y. Lee, S. C. Jeon, J. S. Kim, K. N. Kim, M. S. Hyun, J. J. Yoo, and J. W. Kim, J. Vac. Sci. Technol. B **27**, 2580 (2009).
[5]Q. Dai, S.-Y. Lee, S.-H. Lee, B.-G. Kim, and H.-K. Cho, J. Vac. Sci. Technol. B **30**, 06F307 (2012).
[6]C. Klein, H. Loeschner, and E. Platzgummer, J. Micro/Nanolithogr. MEMS MOEMS **11**, 031402 (2012).
[7]H. Fragner and E. Platzgummer, U.S. patent 7777201 B2 (17 August 2010).
[8]H. Fragner, E. Platzgummer, R. Nowak, and A. Bürli, U.S. patent 8222621 B2 (17 July 2012).
[9]H. Matsumoto, H. Inoue, H. Yamashita, H. Morita, S. Hirose, M. Ogasawara, H. Yamada, and K. Hattori, Proc. SPIE **9984**, 998405 (2016).
[10]P. Petric, C. Bevis, A. Carroll, H. Percy, M. Zywno, K. Standiford, A. Brodie, N. Bareket, and L. Grella, J. Vac. Sci. Technol. B **27**, 161 (2009).
[11]T. Kamikubo, K. Ohtoshi, S. Golladay, V. Katsap, R. Kendall, H. Sunaoshi, and S. Tamamushi, Phys. Procedia **1**, 119 (2008).
[12]C. Tang, M. Su, and Y. Lu, J. Micro/Nanolithogr. MEMS MOEMS **14**, 031212 (2015).
[13]Q. Dai, R. Guo, S.-Y. Lee, J. Choi, S.-H. Lee, I.-K. Shin, and C.-U. Jeon, Microelectron. Eng. **127**, 86 (2014).
[14]S. Johnson, "Simulation of electron scattering in complex nanostructures: Lithography, metrology and characterization," Ph.D. dissertation (Cornell University, 1992).